Electronic Supplementary Information

A Cavitand-based Supramolecular Artificial Light-harvesting System with Two-step Sequential Energy Transfer for Photocatalysis

Qian Liu, Minzan Zuo, Kaiya Wang* and Xiao-Yu Hu*

College of Materials Science and Technology, Nanjing University of Aeronautics and Astronautics, Nanjing 211106, China
Corresponding Author: Kaiya Wang, kwang6@nuaa.edu.cn; Xiao-Yu Hu, huxy@nuaa.edu.cn

Table of Contents

1. General information and experimental procedure

All commonly available reagents and solvents were purchased from Energy Chemical Reagent Co., Ltd. without further purification, and the commercially available reagents and solvents were either employed as purchased or dried according to procedures described in the literature. Column chromatography was performed with silica gel (200 - 400 mesh) produced by Shanghai Titan Scientific Co. Ltd. All yields were given as isolated yields. The NMR spectra were recorded on a Bruker Avance 400 MHz spectrometer with internal standard tetramethylsilane (TMS) and solvent signals as internal references at room temperature, and the chemical shifts (δ) were reported in ppm. UV-vis spectra were followed on a Shimadzu UV 1780 UV-Vis Spectrophotometer. The excitation and emission spectra were recorded on a Hitachi F-7000 Fluorescence Spectrometer. High-resolution electrospray ionization mass spectra (HR-ESI-MS) were recorded on an Agilent Q-TOF 6540 LCMS equipped with an electrospray ionization (ESI) probe operating in the positive-ion mode with direct infusion. Dynamic light scattering (DLS) measurements were carried out on a Brookhaven BI-9000AT system (Brookhaven Instruments Corporation, USA), using a 200 mW polarized laser source (λ = 514 nm). The fluorescence lifetimes were measured employing time-correlated single photon counting on a FLS980 instrument (Edinburg Instruments Ltd., Livingstone, UK) with a pulsed xenon lamp. The quantum yields were carried out on a FLS980 instrument with the integrating sphere.

2. Synthesis of host molecule H and guest molecule TPEG

1) Synthesis of host molecule H

The synthesis of **H** was performed according to the reported literature.[1]

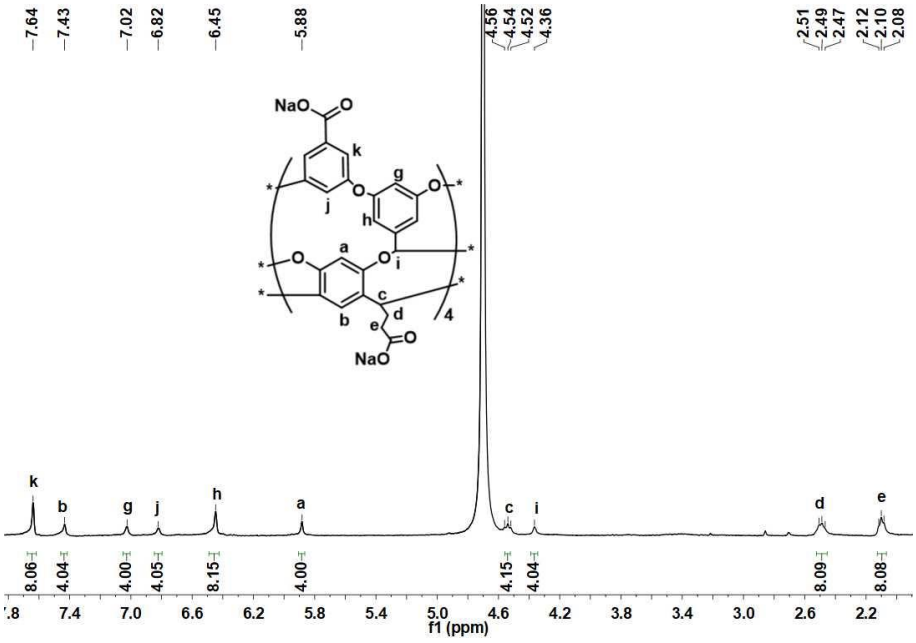

Fig. S1 ^{1}H NMR spectrum (400 MHz, D_2O, 298 K) of **H**.

2) Synthesis of guest molecule TPEG

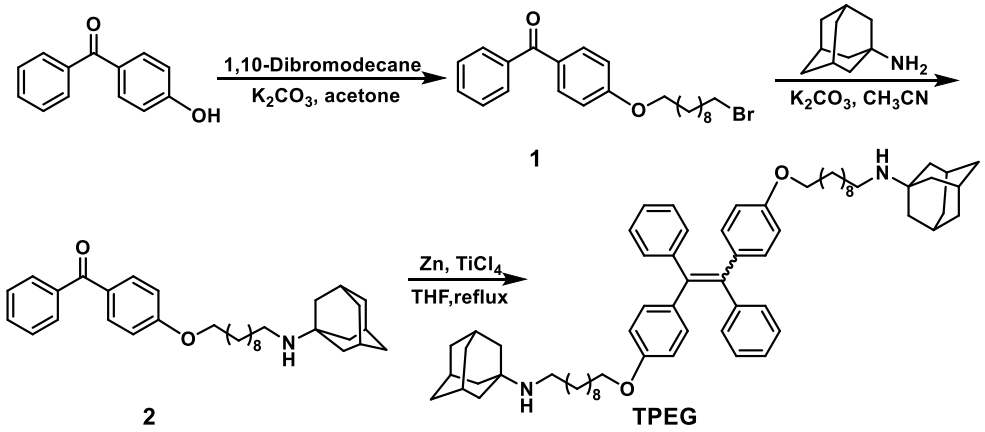

Scheme S1 Synthesis route of guest molecule **TPEG**.

Synthesis of compound 1[2]: 4-Hydroxybenzophenone (2.5 g, 12.6 mmol, 1 equiv.) and K_2CO_3 (4.36 g, 31 mmol, 2.5 equiv.) was dissolved in acetone (35 mL) and stirred for 1 h. Then, the solution of 1, 10-dibromodecane (9.46 g, 31.5 mmol, 2.5 equiv.) in acetone (10 mL) was added dropwise into the above mixture. The mixture was refluxed overnight. After the reaction mixture was cooled to room temperature, the inorganic salt was filtered and washed with acetone three times. The solvent was then removed under reduced pressure and the residue was extracted with chloroform (3 × 60 mL). The organic phase was dried over Na_2SO_4, filtered and concentrated. The crude product was purified by silica gel chromatography (petroleum ether/ethyl acetate = 20:1, *v/v*) to afford compound **1** (4 g, 9.6 mmol, 76%). ^{1}H NMR (400 MHz, $CDCl_3$, 298 K) δ 7.82 (d, *J* = 8.1 Hz, 2H), 7.75 (d, *J* = 7.6 Hz, 2H), 7.59 - 7.53 (m, 1H), 7.47 (t, *J* = 7.4 Hz, 2H), 6.95 (d, *J* = 8.2 Hz, 2H), 4.04 (t, *J* = 6.4 Hz, 2H), 3.41 (t, *J* = 6.7 Hz, 2H), 1.90 - 1.77 (m, 4H), 1.50 - 1.30 (m, 12H).

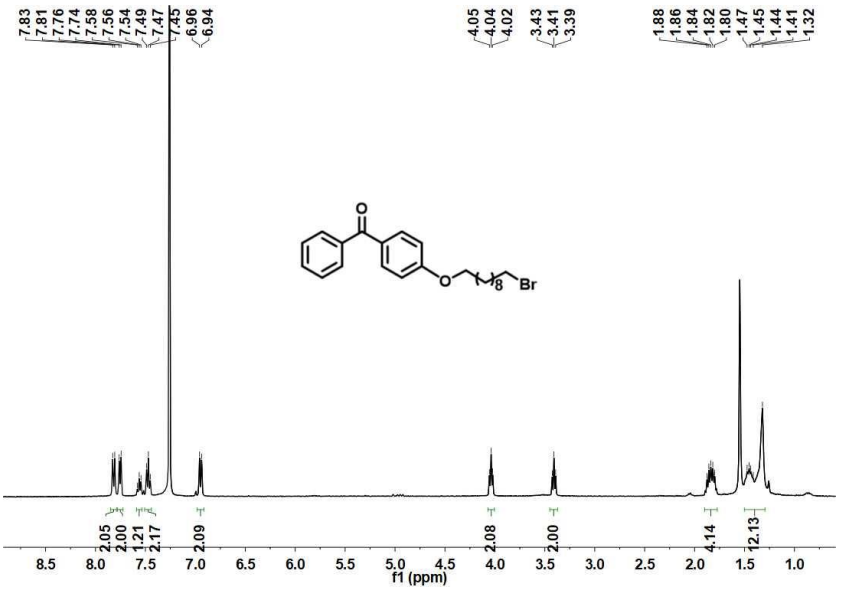

Fig. S2 ^{1}H NMR spectrum (400 MHz, $CDCl_3$, 298 K) of compound **1**.

Synthesis of compound 2: Compound **1** (1.04 g, 2.5 mmol, 1 equiv.), 1-adamantanamine (945 mg, 6.25 mmol, 2.5 equiv.) and K_2CO_3 (6.9 g, 50 mmol, 20 equiv.) were dissolved in CH_3CN (30 mL). Under nitrogen atmosphere, the mixture was refluxed for one day. The solvent was removed under reduced pressure and the residue was purified by silica gel column chromatography (dichloromethane/methanol = 50:1, *v/v*) to afford compound **2** (366 mg, 0.75 mmol, 30%). ^{1}H NMR (400 MHz, $CDCl_3$, 298 K) δ 7.82 (d, *J* = 8.1 Hz, 2H), 7.75 (d, *J* = 8.0 Hz, 2H), 7.56 (t, *J* = 7.3 Hz, 1H), 7.47 (t, *J* = 7.6 Hz, 2H), 6.95 (d, *J* = 8.2 Hz, 2H), 4.03 (t, *J* = 6.4 Hz, 2H), 2.61 (t, *J* = 7.2 Hz, 2H), 2.08 (s, 3H), 1.80 (m, *J* = 14.3, 6.9 Hz, 2H), 1.75 - 1.61 (m, 12H), 1.51 - 1.23 (m, 14H). ^{13}C NMR (100 MHz, $CDCl_3$, 298 K) δ 195.57, 162.89, 138.40, 132.57, 131.82, 129.82, 128.17, 114.03, 68.30, 42.49, 40.42, 36.72, 30.83, 29.59, 29.34, 29.13, 27.53, 25.99. HR-ESI-MS m/z: $[M + H]^+$ calcd for $[C_{33}H_{46}NO_2]^+$, 488.3529; found, 488.3530.

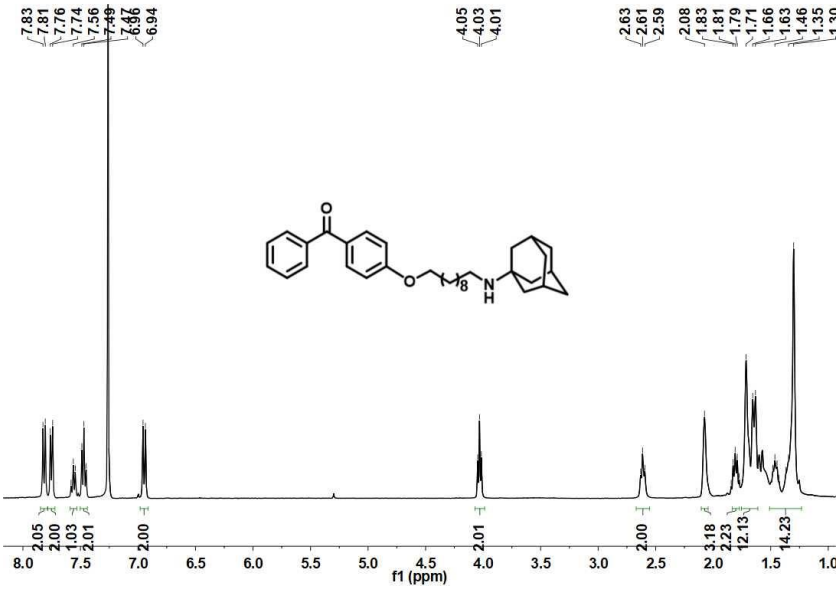

Fig. S3 ^{1}H NMR spectrum (400 MHz, $CDCl_3$, 298 K) of compound **2**.

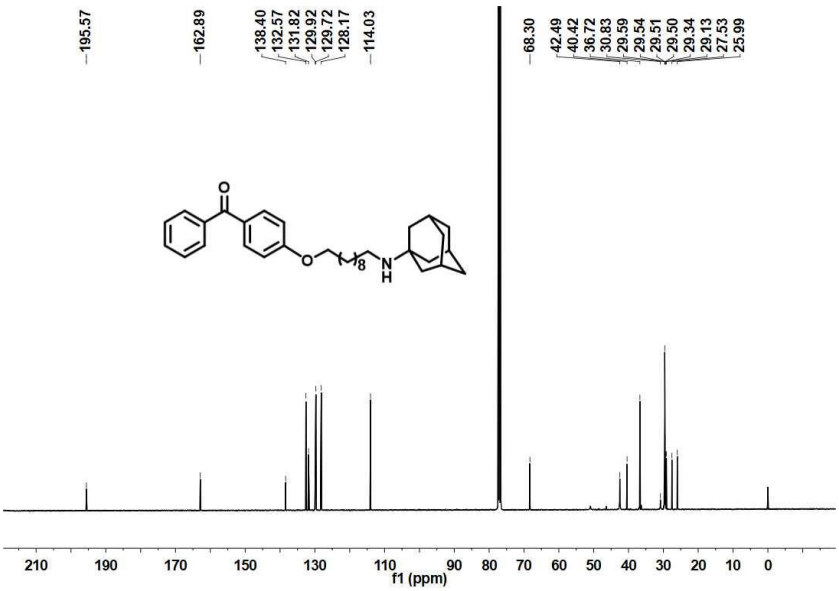

Fig. S4 ^{13}C NMR spectrum (100 MHz, $CDCl_3$, 298 K) of compound **2**.

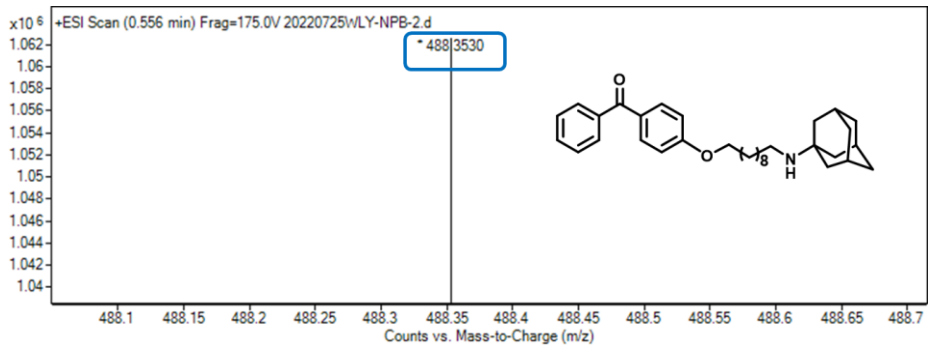

Fig. S5 HR-ESI-MS spectrum of compound **2**.

Synthesis of compound TPEG: Compound **2** (675 mg, 1.34 mmol,1 equiv.) and zinc dust (438 g, 6.7 mmol, 5 equiv.) were placed in THF (15 mL). Under nitrogen atmosphere, the mixture was cooled to –20 ℃ and $TiCl_4$ (0.32 mL, 2.68 mmol, 2 equiv.) was added slowly. Then the mixture was refluxed overnight. The mixture was quenched with saturated aqueous $NaHCO_3$ solution and filtered. The filtrate was extracted with dichloromethane. The organic layer was washed with water and dried over Na_2SO_4. The solvent was removed under reduced pressure and the crude product was purified by silica gel column chromatography (dichloromethane/methanol = 10:1, *v*/*v*) to afford compound **TPEG**. ^{1}H NMR (400 MHz, $CDCl_3$, 298 K) δ 7.07 (t, *J* = 6.5 Hz, 6H), 7.04 - 7.00 (m, 4H), 6.87 (d, *J* = 8.6 Hz, 4H), 6.58 (d, *J* = 8.7 Hz, 4H), 3.83 (t, *J* = 6.5 Hz, 4H), 2.80 - 2.74 (m, 4H), 2.13 (s, 4H), 2.05 (s, 2H), 1.97 (s, 12H), 1.85 (s, 2H), 1.68 (s, 8H), 1.61 (s, 4H), 1.39 (dd, *J* = 14.4, 5.7 Hz, 4H), 1.25 (dd, *J* = 17.7, 10.9 Hz, 28H). ^{13}C NMR (100 MHz, $CDCl_3$, 298 K) δ 157.51, 144.37, 139.63, 136.19, 132.53, 131.41, 127.63, 126.11, 113.56, 67.75, 57.43, 52.95, 40.67, 40.10, 38.50, 35.62, 35.37, 29.06, 28.98, 27.25, 26.69, 26.07. HR-ESI-MS m/z: $[M + H]^+$ calcd for $[C_{66}H_{91}N_2O_2]^+$, 943.7081; found, 943.7081.

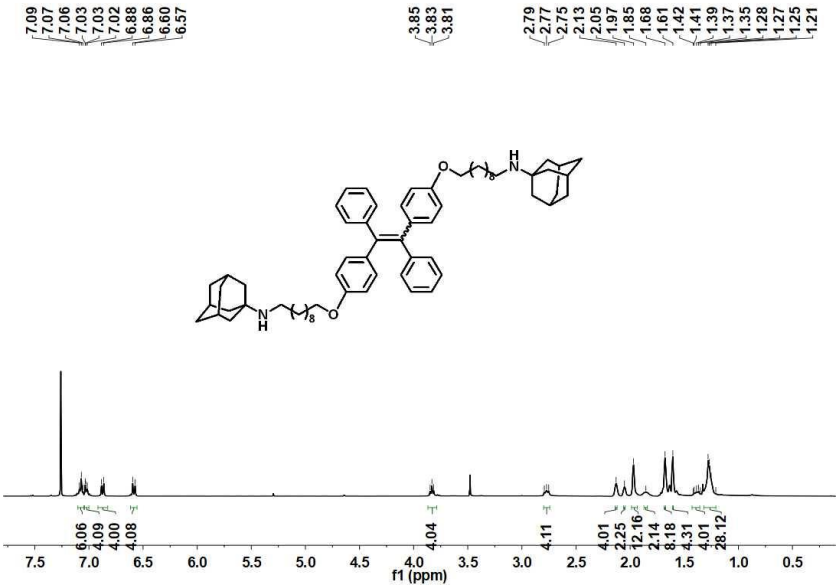

Fig. S6 ^{1}H NMR spectrum (400 MHz, $CDCl_3$, 298 K) of compound **TPEG**.

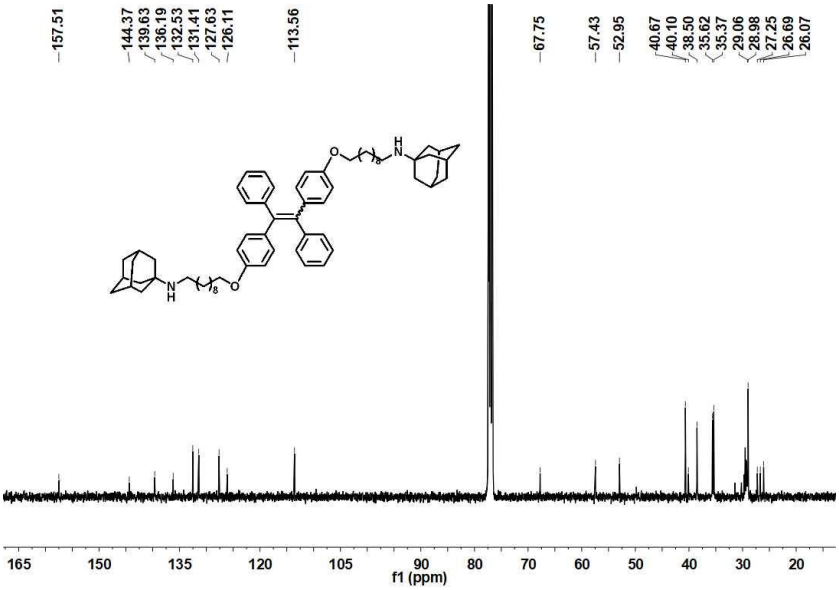

Fig. S7 ^{13}C NMR spectrum (100 MHz, $CDCl_3$, 298 K) of compound **TPEG**.

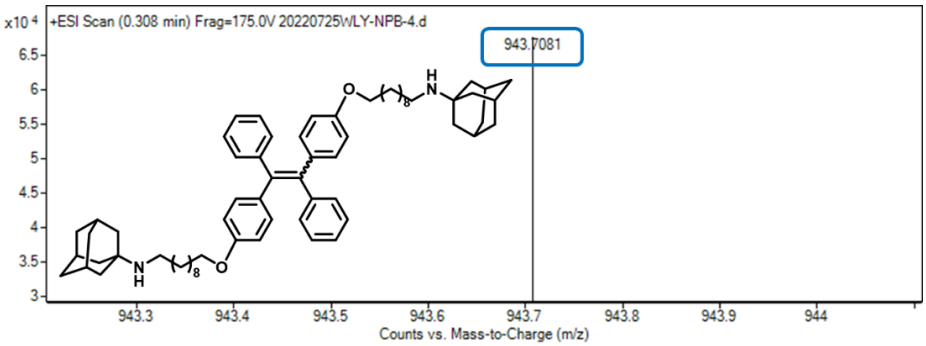

Fig. S8 HR-ESI-MS spectrum of compound **TPEG**.

3. Host-guest interaction of H and TPEG

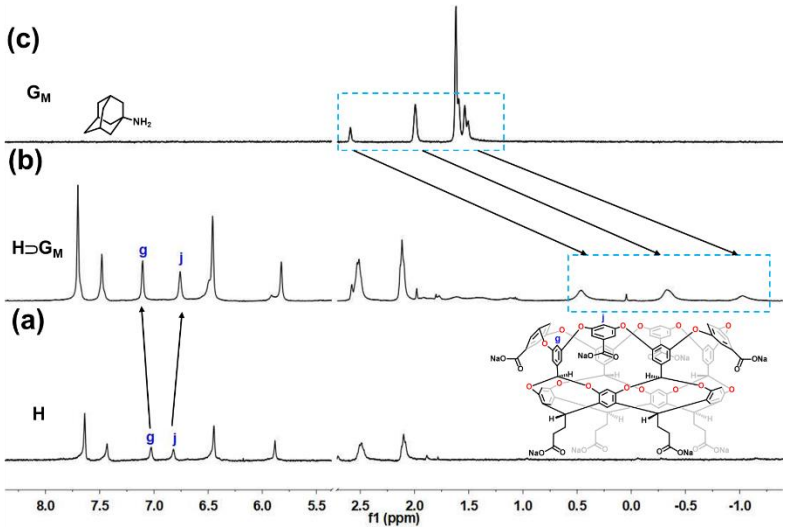

Fig. S9 Partial ^{1}H NMR spectra (400 MHz, $CDCl_3$, 298 K) of (a) **H**; (b) **H**⊃**G**$_\mathbf{M}$; (c) **G**$_\mathbf{M}$. [**H**] = 2 mM, [**G**$_\mathbf{M}$] = 2 mM.

4. AIE properties of TPEG

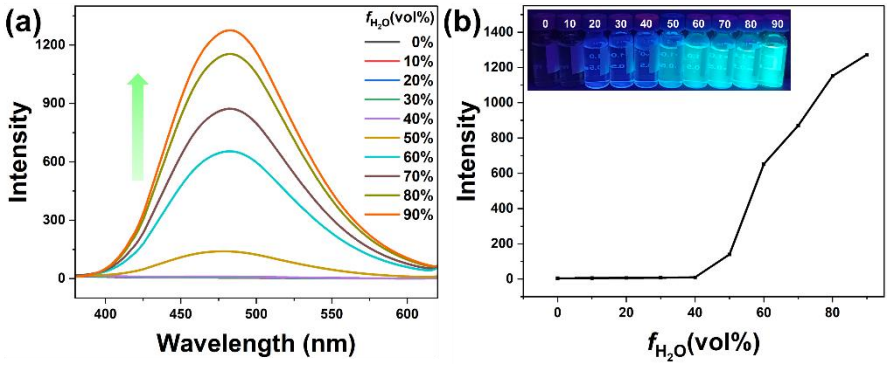

Fig. S10 (a) Fluorescence spectra of **TPEG** in water-methanol mixture with different water contents; (b) Plot of maximum emission intensity of **TPEG**. The inset: fluorescence images of **TPEG** with different water content under UV light irradiation. [**TPEG**] = 5 × 10^{-5} M.

5. Self-assembly of H and TPEG, H and TPEG with acceptors

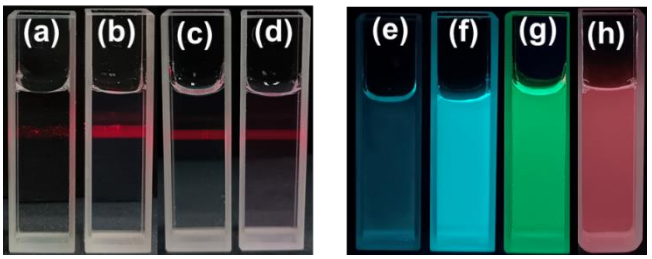

Fig. S11 The Tyndall effect of (a) free **TPEG**, (b) **H⊃TPEG** assembly, (c) **H⊃TPEG-EsY** assembly, (d) **H⊃TPEG-EsY-NiR** assembly; Photographs of (e) free **TPEG**, (f) **H⊃TPEG** assembly, (g) **H⊃TPEG-EsY** assembly, (h) **H⊃TPEG-EsY-NiR** assembly under UV lamp irradiation. [**H**] = 1 × 10^{-5} M, [**TPEG**] = 7 × 10^{-5} M, [**EsY**] = 3.5 × 10^{-7} M, [**NiR**] = 3.5 × 10^{-7} M.

6. Determination of the best molar ratio between H and TPEG

The best molar ratio of **H** and **TPEG** for the construction of supramolecular self-assemblies can be determined by transmittance experiments. Upon addition of **H** into the aqueous solution of **TPEG**, the optical transmittance of the system at 400 nm decreased sharply to the minimum, and then increased again, which indicated the formation of more compact aggregates at the inflection point. It represents the best molar ratio of **H** and **TPEG** for the construction of supramolecular assemblies ([**H**]/[**TPEG**] = 1:7).

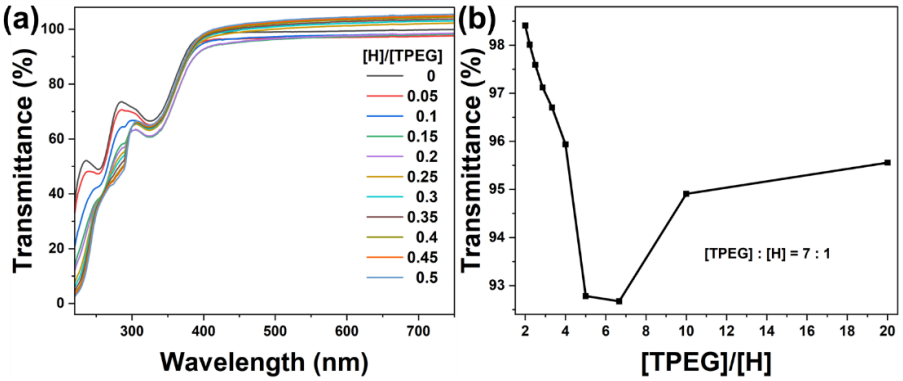

Fig. S12 (a) Optical transmittance of a mixture of **H** and **TPEG** in water with a constant **TPEG** concentration (0.02 mM) and varying concentration of **H** (from 0.05 to 0.5 equiv.) at 25 °C; (b) Dependence of the relative optical transmittance at 400 nm on the **H** concentration with a fixed concentration of **TPEG** (0.02 mM) at 25 °C.

7. Determination of the critical aggregation concentration (CAC) for H and TPEG

At the best molar ratio, the transmittance of the system gradually decreases as the concentration increases. The inflection point is the critical aggregation concentration, indicating that a large number of nanoparticles will be formed above this concentration. The critical aggregation concentration (CAC) of this system was determined to be 0.013 mM.

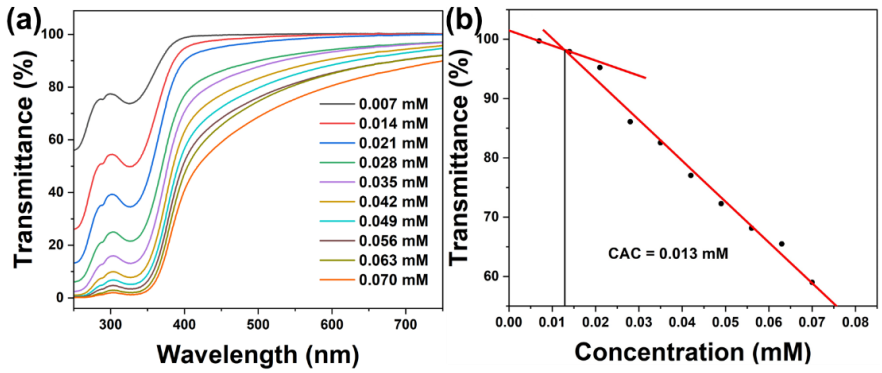

Fig. S13 Optical transmittance of a mixture of **H** and **TPEG** in water with the best molar ratio of **H** and **TPEG** ([**TPEG**]/[**H**] = 7:1) upon increasing the concentration of **TPEG** (0.007 mM - 0.07 mM) at 25 °C.

8. DLS data of the assembly

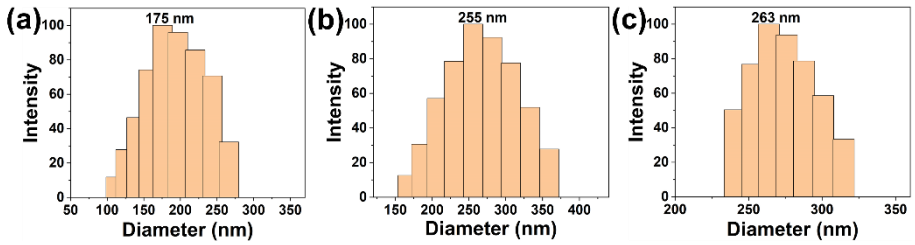

Fig. S14 DLS data of (a) **H⊃TPEG** assembly, (b) **H⊃TPEG-EsY** assembly, and (c) **H⊃TPEG-EsY-NiR** assembly in water.

9. Overlap between the fluorescent emission of assembly and the absorption of dyes

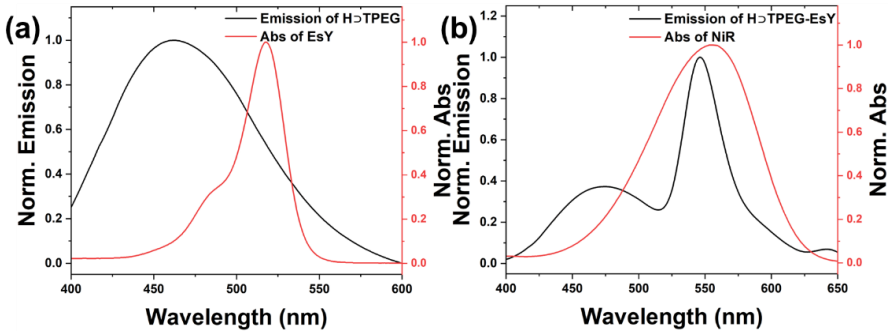

Fig. S15 (a) Normalized emission spectrum of **H⊃TPEG** assembly upon excitation at 365 nm and normalized absorption spectrum of EsY in water; (b) Normalized emission spectrum of **H⊃TPEG-EsY** assembly upon excitation at 365 nm and normalized absorption spectrum of NiR in water.

10. Quantum yields and fluorescence lifetime measurements

To further verify the occurrence of the light-harvesting process, fluorescence quantum yields and fluorescence decay experiments were performed. The fluorescence lifetimes were fitted as a double exponential decay. The results showed that the quantum yields and the lifetime of the nanoparticles gradually decreased with the loading of dyes, suggesting that the **H⊃TPEG** assemblies could serve as an efficient light-harvesting system to transfer the captured energy first to EsY and then to NiR.

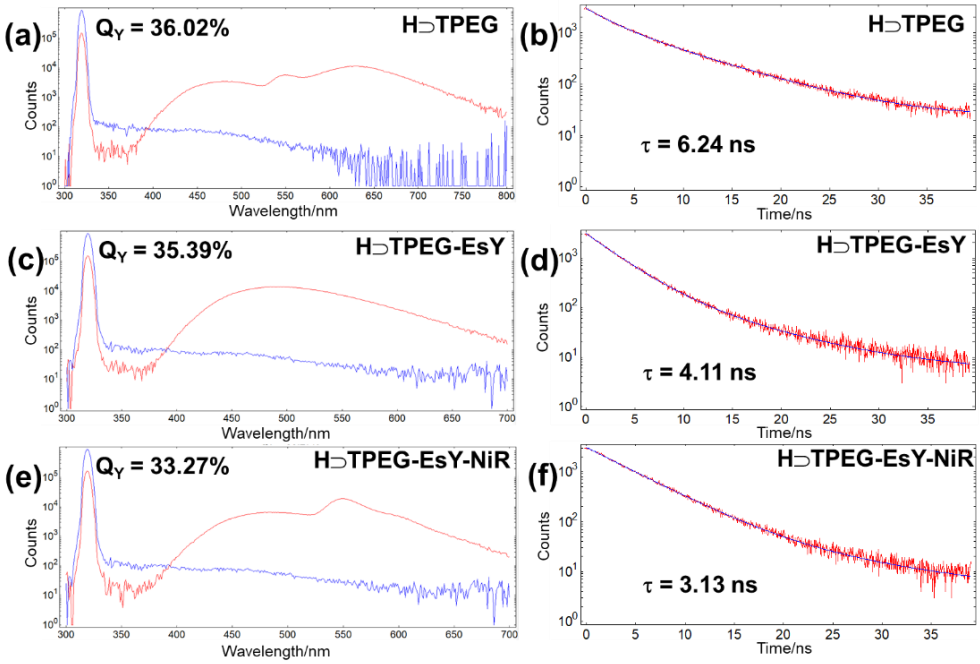

Fig. S16 Absolute fluorescence quantum yields ($\Phi_{f(Abs)}$) of (a) **H⊃TPEG** assembly, (c) **H⊃TPEG -ESY** assembly, and (e) **H⊃TPEG-ESY-NiR** assembly upon excitation at 365 nm in aqueous solution. Fluorescence decay profiles of (b) **H⊃TPEG** assembly monitored at 480 nm, (d) **H⊃TPEG-EsY** assembly monitored at 550 nm, and (f) **H⊃TPEG-EsY-NiR** assembly monitored at 620 nm upon excitation at 365 nm in aqueous solution. [**H**] = 1×10^{-5} M, [**TPEG**] = 7×10^{-5} M, [**EsY**] = 3.5×10^{-7} M, [**NiR**] = 3.5×10^{-7} M.

Table S1 Quantum yields and fluorescence lifetimes of **H⊃TPEG** assembly, **H⊃TPEG-EsY** assembly, and **H⊃TPEG-EsY-NiR** assembly. [**H**] = 1×10^{-5} M, [**TPEG**] = 7×10^{-5} M, [**EsY**] = 3.5×10^{-7} M, [**NiR**] = 3.5×10^{-7} M.

Sample	τ_1/ns	RW_1[%]	τ_2/ns	RW_2[%]	τ/ns	χ^2	Q_Y (%)
H⊃TPEG	2.57	23.02	7.34	76.98	6.24	0.9637	36.02%
H⊃TPEG-EsY	2.91	76.12	7.92	23.88	4.11	1.0762	35.39%
H⊃TPEG-EsY –NiR	1.43	48.15	4.72	51.85	3.13	1.19	33.27%

11. Energy-transfer efficiency and antenna effect calculations

1) Energy-transfer efficiency and antenna effect of H⊃TPEG assembly to EsY

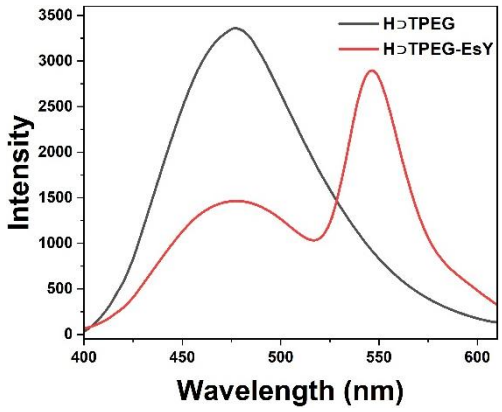

Fig. S17 Fluorescence spectra of **H⊃TPEG** and **H⊃TPEG-EsY** assembly upon excitation at 365 nm. [**H**] = 1×10^{-5} M, [**TPEG**] = 7×10^{-5} M, [**EsY**] = 3.5×10^{-7} M.

Energy-transfer efficiency (Φ_{ET}) was calculated from excitation fluorescence spectra through the equation S1:

$$\Phi_{ET} = 1 - I_{DA} / I_D \quad \text{(eq. S1)}$$

Where I_{DA} and I_D are the fluorescence intensities of the emission of **H⊃TPEG-EsY** assembly (donor and acceptor) and **H⊃TPEG** assembly (donor) respectively when excited at 365 nm.

The energy-transfer efficiency (Φ_{ET}) was calculated as 57% in aqueous environment, measured under the condition of [**H**] = 1×10^{-5} M, [**TPEG**] = 7×10^{-5} M, [**EsY**] = 3.5×10^{-7} M and λ_{ex} = 365 nm.

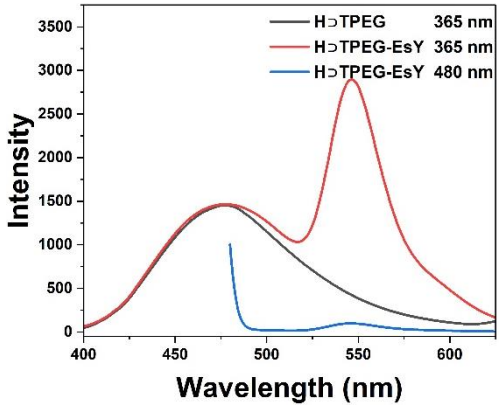

Fig. S18 Fluorescence spectra of **H⊃TPEG-EsY** in water (red line), blue line (acceptor emission, λ_{ex} = 480 nm). The black line represents the fluorescence spectrum of **H⊃TPEG**, which was normalized according to the fluorescence intensity at 480 nm of the red line. [**H**] = 1×10^{-5} M, [**TPEG**] = 7×10^{-5} M, [**EsY**] = 3.5×10^{-7} M.

The antenna effect (AE) was calculated based on the excitation spectra using equation S2.

$$\mathbf{AE = (I_{DA,365} - I_{D,365}) / I_{DA,480}} \text{ (eq. S2)}$$

Where $I_{DA,365}$ and $I_{DA,480}$ are the fluorescence intensities at 550 nm with the excitation of the donor at 365 nm and the direct excitation of the acceptor at 480 nm, respectively. $I_{D,365}$ is the fluorescence intensity at 550 nm of the **H⊃TPEG** assembly, which was normalized with the **H⊃TPEG-EsY** assembly at 480 nm.

The antenna effect value was calculated as 25.8 in water, measured under the condition of [**H**] = 1 × 10^{-5} M, [**TPEG**] = 7 × 10^{-5} M, [**EsY**] = 3.5 × 10^{-7} M.

2) Energy-transfer efficiency and antenna effect of H⊃TPEG-EsY assembly to NiR

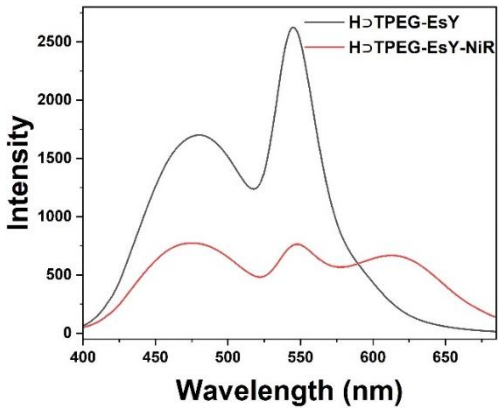

Fig. S19 Fluorescence spectra of **H⊃TPEG-EsY** and **H⊃TPEG-EsY-NiR** assembly upon excitation at 365 nm. [**H**] = 1 × 10^{-5} M, [**TPEG**] = 7 × 10^{-5} M, [**EsY**] = 3.5 × 10^{-7} M, [**NiR**] = 3.5 × 10^{-7} M.

Energy-transfer efficiency (Φ_{ET}) was calculated from excitation fluorescence spectra through the equation S3:

$$\mathbf{\Phi_{ET} = 1 - I_{DA} / I_D} \text{ (eq. S3)}$$

Where I_{DA} and I_D are the fluorescence intensities of the emission of **H⊃TPEG-EsY-NiR** assembly (donor and acceptor) and **H⊃TPEG-EsY** assembly (donor) respectively when excited at 365 nm.

The energy-transfer efficiency (Φ_{ET}) was calculated as 71% in aqueous environment, measured under the condition of [**H**] = 1 × 10^{-5} M, [**TPEG**] = 7 × 10^{-5} M, [**EsY**] = 3.5 × 10^{-7} M, [**NiR**] = 3.5 × 10^{-7} M and λ_{ex} = 365 nm.

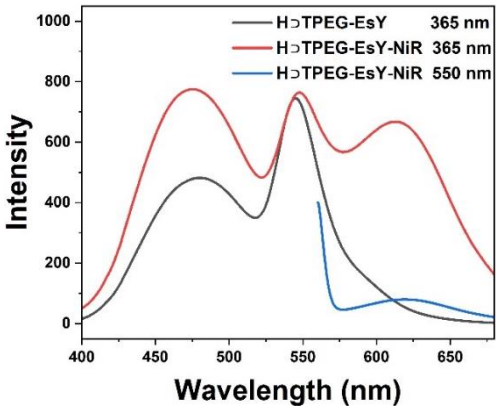

Fig. S20 Fluorescence spectra of **H⊃TPEG-EsY-NiR** in water (red line), blue line (acceptor emission, λ_{ex} = 550 nm). The black line represents the fluorescence spectrum of **H⊃TPEG-EsY**, which was normalized according to the fluorescence intensity at 550 nm of the red line. [**H**] = 1 × 10^{-5} M, [**TPEG**] = 7 × 10^{-5} M, [**EsY**] = 3.5 × 10^{-7} M, [**NiR**] = 3.5 × 10^{-7} M.

The antenna effect (AE) was calculated based on the excitation spectra using equation S4.

$$\mathbf{AE = (I_{DA,365} - I_{D,365}) / I_{DA,550}}\ \text{(eq. S4)}$$

Where $I_{DA,365}$ and $I_{DA,550}$ are the fluorescence intensities at 620 nm with the excitation of the donor at 365 nm and the direct excitation of the acceptor at 550 nm, respectively. $I_{D,365}$ is the fluorescence intensity at 620 nm of the **H⊃TPEG-EsY** assembly, which was normalized with the **H⊃TPEG-EsY-NiR** assembly at 550 nm.

The antenna effect value was calculated as 7.5 in water, measured under the condition of [**H**] = 1 × 10^{-5} M, [**TPEG**] = 7 × 10^{-5} M, [**EsY**] = 3.5 × 10^{-7} M, [**NiR**] = 3.5 × 10^{-7} M.

12. The electron transfer process and trapping experiments of $O_2^{\bullet-}$

The electron transfer process could be confirmed by the titration of *N*-phenyl-1, 2, 3, 4-tetrahydroisoquinoline into the **H⊃TPEG-EsY-NiR** assembly with fluorescence spectra.[3] The addition of *N*-phenyl-1, 2, 3, 4-tetrahydroisoquinoline resulted in a decrease in the fluorescent intensity of the **H⊃TPEG-EsY-NiR** assembly, indicating the occurrence of electron transfer.

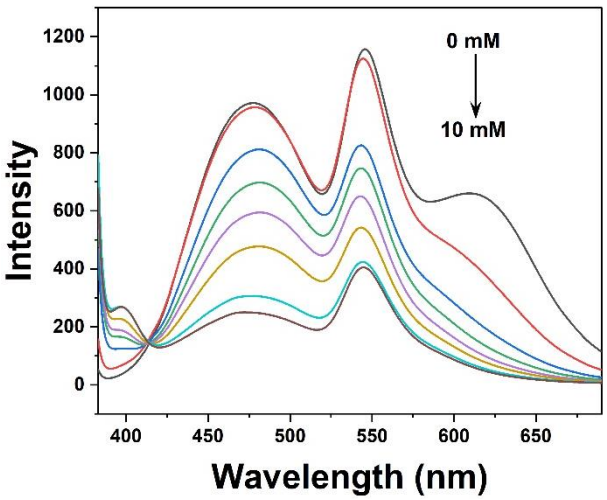

Fig. S21 Fluorescence emission spectra of **H⊃TPEG-EsY-NiR** system in water with the addition of *N*-phenyl-1, 2, 3, 4-tetrahydroisoquinoline upon excitation at 365 nm. [**H**] = 1×10^{-5} M, [**TPEG**] = 7×10^{-5} M, [**EsY**] = 3.5×10^{-7} M, [**NiR**] = 3.5×10^{-7} M.

According to the reference,[4] Rhodamine B (RhB) can undergo degradation by both $O_2^{\bullet-}$ and $^1O_2$ species. As shown in the **Fig.** S22, the absorption of RhB at 550 nm exhibited a significant decrease in the presence of **H⊃TPEG-EsY-NiR** and *N*-phenyl-1, 2, 3, 4-tetrahydroisoquinoline, indicating efficient ROS production. Furthermore, upon addition of 1, 4-benzoquinone (a specific $O_2^{\bullet-}$ quencher) under identical conditions, the absorption of RhB remained almost unchanged, suggesting the predominant ROS is $O_2^{\bullet-}$ in this system.

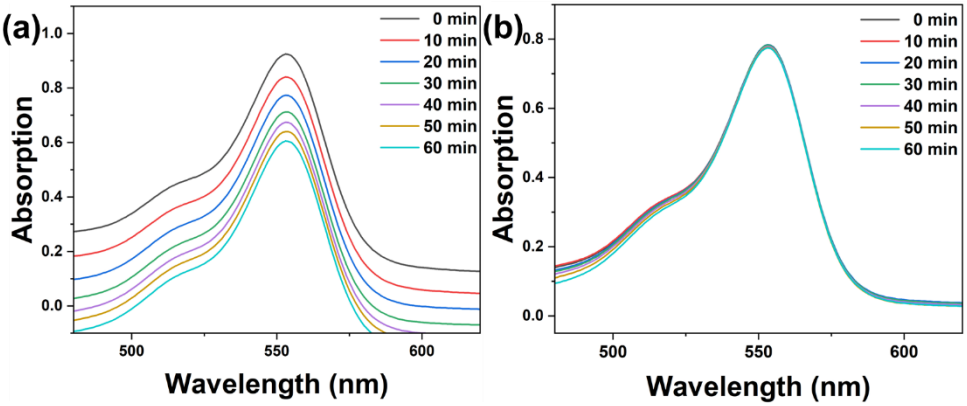

Fig. S22 The absorption spectra of RhB (50 μM) in the presence of (a) **H⊃TPEG-EsY-NiR** and *N*-phenyl-1, 2, 3, 4-tetrahydroisoquinoline (10 μM); (b) **H⊃TPEG-EsY-NiR**, *N*-phenyl-1, 2, 3, 4-tetrahydroisoquinoline (10 μM) and 1, 4-benzoquinone (100 μM) after irradiation (white light) for different time.

Nitro blue tetrazolium (NBT) is widely utilized as a probe for the detection of $O_2^{\bullet-}$, which forms formazan (a blue/violet colored precipitate) upon capturing $O_2^{\bullet-}$.[5] Herein, upon addition of **H⊃TPEG-EsY-NiR** and *N*-phenyl-1, 2, 3, 4-tetrahydroisoquinoline into NBT solution, the formation of precipitate could be observed after irradiation.

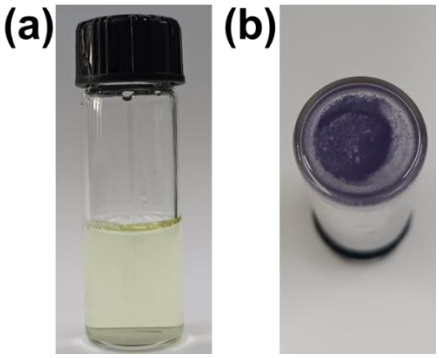

Fig. S23 (a) The aqueous solution of NBT; (b) The precipitate formazan after the addition of **H⊃TPEG-EsY-NiR** and *N*-phenyl-1, 2, 3, 4-tetrahydroisoquinoline under irradiation.

13. H⊃TPEG-EsY-NiR system for the photocatalytic reaction in aqueous medium

1) Synthesis of *N*-phenyl-1, 2, 3, 4-tetrahydroisoquinoline and its derivatives

Synthesis of *N*-phenyl-1, 2, 3, 4-tetrahydroisoquinoline: CuI (200 mg, 1 mmol, 0.1 equiv.) and K_3PO_4 (4.25 g, 20 mmol, 2 equiv.) were added to a flask under nitrogen atmosphere. 2-propanol (10 mL), ethylene glycol (11 mL), 1, 2, 3, 4-tetrahydroisoquinoline (2 mL, 15 mmol, 1.5 equiv.), and iodobenzene (1.12 mL, 10 mmol, 1 equiv.) were added in turn and then reacted at 90 ℃ for 24 h. After the reaction, the mixture was cooled to room temperature and water (25 mL) was added. Then the mixture was extracted with ethyl acetate. The organic phases were combined, washed with brine, and dried over Na_2SO_4. The solvent was removed under reduced pressure, and the crude product was purified by silica gel column chromatography (petroleum ether) to afford the pure product as a light-yellow solid (0.7 g, 3.3 mmol, 33%). ^{1}H NMR (400 MHz, $CDCl_3$, 298 K) δ 7.33 - 7.27 (m, 2H), 7.21 - 7.15 (m, 4H), 7.01 (d, J = 7.9 Hz, 2H), 6.85 (t, J = 7.0 Hz, 1H), 4.42 (s, 2H), 3.58 (t, J = 5.8 Hz, 2H), 3.00 (t, J = 5.7 Hz, 2H).

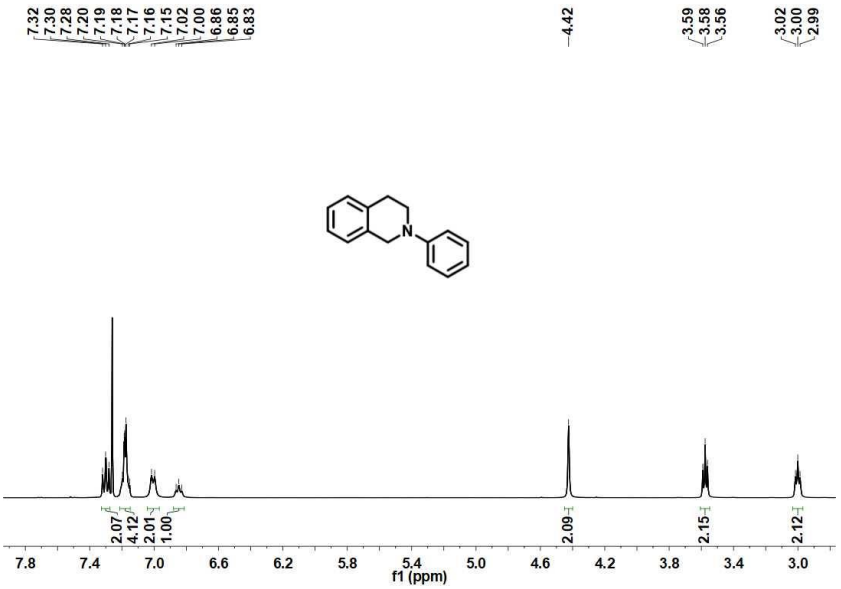

Fig. S24 ^{1}H NMR spectrum (400 MHz, $CDCl_3$, 298 K) of compound *N*-phenyl-1, 2, 3, 4-tetrahydroisoquinoline.

The synthesis of its derivatives is similar to that of *N*-phenyl-1, 2, 3, 4-tetrahydroisoquinoline.

2-(4-methylphenyl)-1, 2, 3, 4-tetrahydroisoquinoline: ^{1}H NMR (400 MHz, $CDCl_3$, 298 K) δ 7.17 (m, J = 9.4, 4.5 Hz, 4H), 7.10 (d, J = 8.3 Hz, 2H), 6.92 (d, J = 8.4 Hz, 2H), 4.36 (s, 2H), 3.51 (t, J = 5.9 Hz, 2H), 2.99 (t, J = 5.8 Hz, 2H), 2.28 (s, 3H).

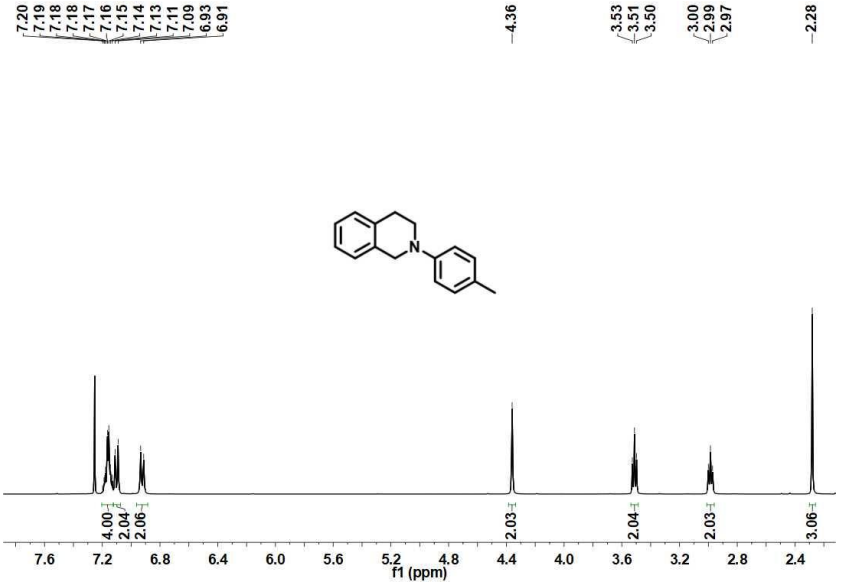

Fig. S25 ^{1}H NMR spectrum (400 MHz, $CDCl_3$, 298 K) of compound 2-(4-methylphenyl)-1, 2, 3, 4-tetrahydroisoquinoline.

2-(4-methoxyphenyl)-1, 2, 3, 4-tetrahydroisoquinoline: ^{1}H NMR (400 MHz, $CDCl_3$, 298 K) δ 7.21 - 7.11 (m, 4H), 7.00 (d, J = 9.0 Hz, 2H), 6.90 - 6.85 (m, 2H), 4.31 (s, 2H), 3.78 (s, 3H), 3.45 (t, J = 5.9 Hz, 2H), 2.99 (t, J = 5.8 Hz, 2H).

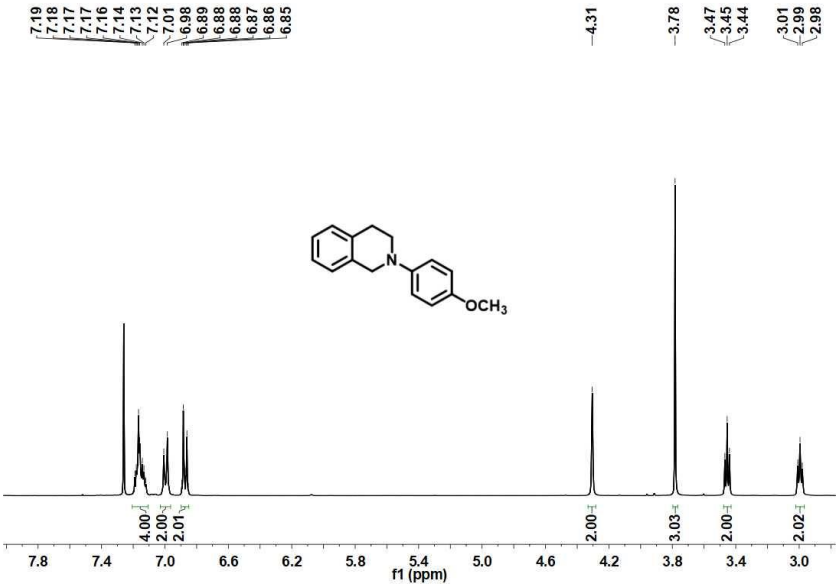

Fig. S26 ^{1}H NMR spectrum (400 MHz, $CDCl_3$, 298 K) of compound 2-(4-methoxyphenyl)-1, 2, 3, 4-tetrahydroisoquinoline.

2-(4-bromophenyl)-1, 2, 3, 4-tetrahydroisoquinoline: ^{1}H NMR (400 MHz, $CDCl_3$, 298 K) δ 7.36 (d, J = 9.0 Hz, 2H), 7.22 - 7.14 (m, 4H), 6.85 (d, J = 8.4 Hz, 2H), 4.38 (s, 2H), 3.54 (t, J = 5.9 Hz, 2H), 2.98 (t, J = 5.8 Hz, 2H).

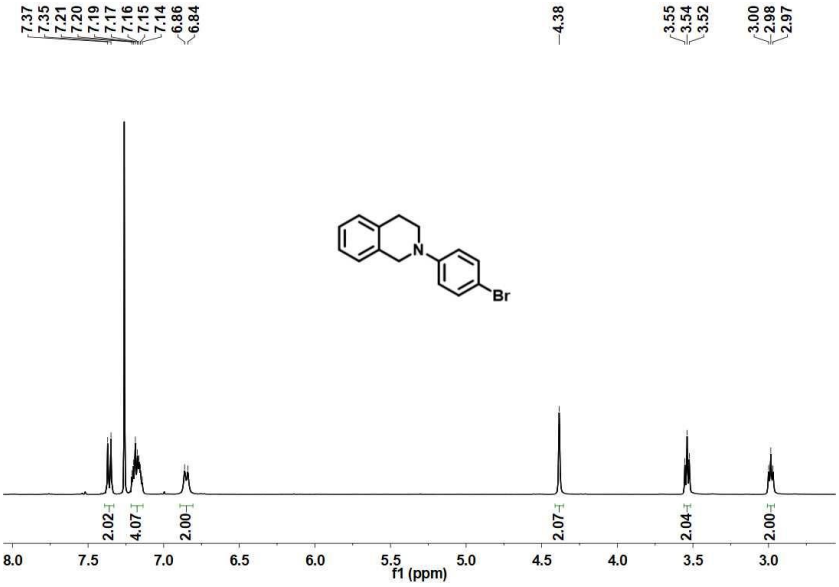

Fig. S27 ^{1}H NMR spectrum (400 MHz, $CDCl_3$, 298 K) of compound 2-(4-bromophenyl)-1, 2, 3, 4-tetrahydroisoquinoline.

2) Yields of the CDC reaction with different substrates

Table S2 Yields of the CDC reaction catalyzed by the **H⊃TPEG-EsY-NiR** system.

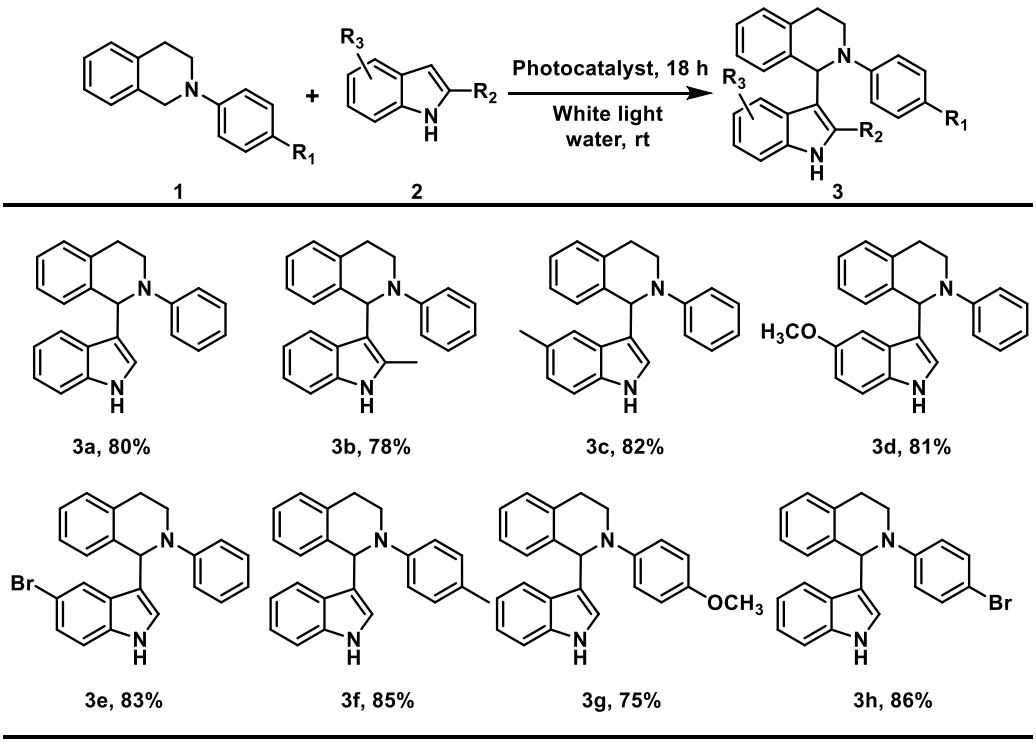

3) ^{1}H NMR data of 3a-3h

3a: ^{1}H NMR (400 MHz, $CDCl_3$, 298 K) δ 7.95 (s, 1H), 7.54 (d, *J* = 8.6 Hz, 1H), 7.37 - 7.31 (m, 2H), 7.25 - 7.21 (m, 2H), 7.16 (dd, *J* = 13.4, 4.6 Hz, 4H), 7.02 (dd, *J* = 13.5, 6.9 Hz, 3H), 6.82 - 6.75 (m, 1H), 6.65 (s, 1H), 6.18 (s, 1H), 3.64 (d, *J* = 1.6 Hz, 2H), 3.08 (dt, *J* = 15.4, 7.6 Hz, 1H), 2.82 (d, *J* = 15.9 Hz, 1H).

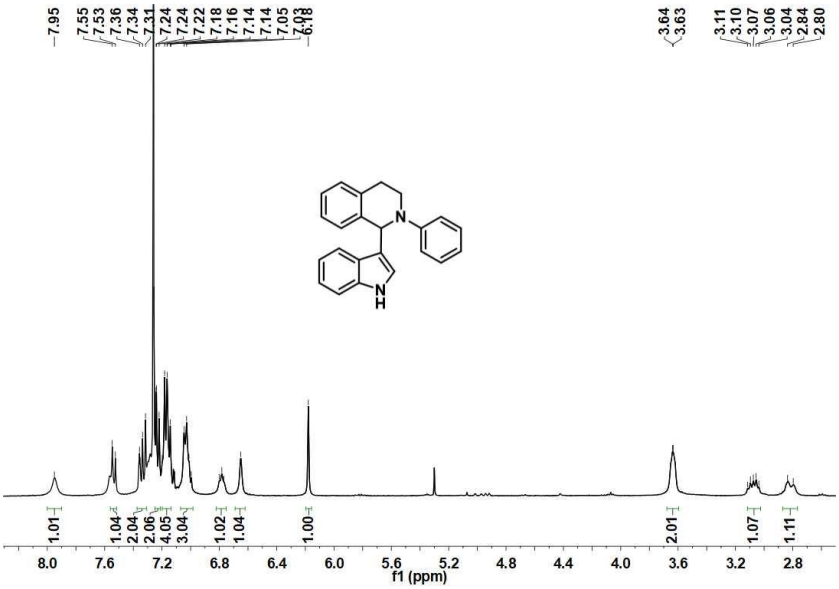

Fig. S28 ^{1}H NMR spectrum (400 MHz, $CDCl_3$, 298 K) of compound **3a**.

3b: ^{1}H NMR (400 MHz, $CDCl_3$, 298 K) δ 7.72 (s, 1H), 7.18 (dd, *J* = 15.4, 8.1 Hz, 5H), 7.07 (dd, *J* = 11.6, 7.4 Hz, 3H), 7.04 - 6.97 (m, 3H), 6.89 (t, *J* = 7.5 Hz, 1H), 6.86 - 6.79 (m, 1H), 5.96 (s, 1H), 3.71 - 3.57 (m, 2H), 3.04 (dd, *J* = 36.4, 16.0 Hz, 2H), 2.02 (s, 3H).

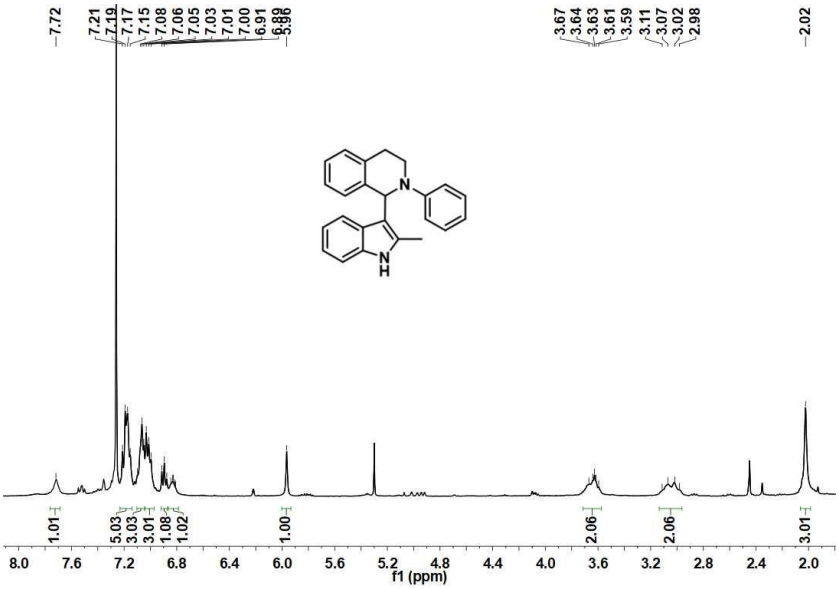

Fig. S29 ^{1}H NMR spectrum (400 MHz, $CDCl_3$, 298 K) of compound **3b**.

3c: ^{1}H NMR (400 MHz, $CDCl_3$, 298 K) δ 7.85 (s, 1H), 7.34 (d, *J* = 13.8 Hz, 2H), 7.23 (d, *J* = 8.4 Hz, 2H), 7.21 - 7.12 (m, 4H), 7.04 (d, *J* = 7.1 Hz, 2H), 6.99 (d, *J* = 8.1 Hz, 1H), 6.84 - 6.75 (m, 1H), 6.57 (s, 1H), 6.14 (s, 1H), 3.64 (s, 2H), 3.12 - 3.02 (m, 1H), 2.80 (d, *J* = 15.5 Hz, 1H), 2.37 (s, 3H).

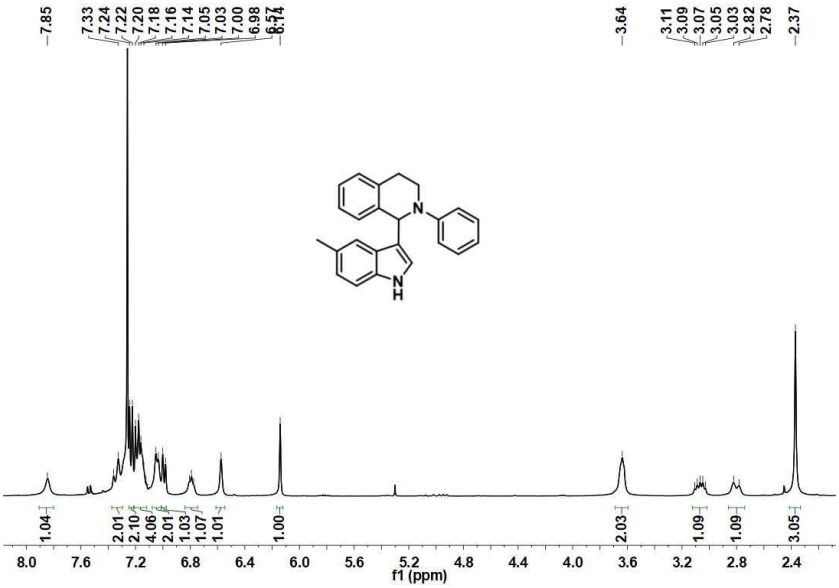

Fig. S30 ^{1}H NMR spectrum (400 MHz, $CDCl_3$, 298 K) of compound **3c**.

3d: ^{1}H NMR (400 MHz, $CDCl_3$, 298 K) δ 7.83 (s, 1H), 7.28 (s, 1H), 7.25 - 7.14 (m, 6H), 7.03 (d, *J* = 7.9 Hz, 2H), 6.88 (s, 1H), 6.83 - 6.75 (m, 2H), 6.59 (s, 1H), 6.15 (s, 1H), 3.66 (s, 3H), 3.64 - 3.57 (m, 2H), 3.08 (dt, *J* = 15.4, 7.6 Hz, 1H), 2.82 (d, *J* =

16.4 Hz, 1H).

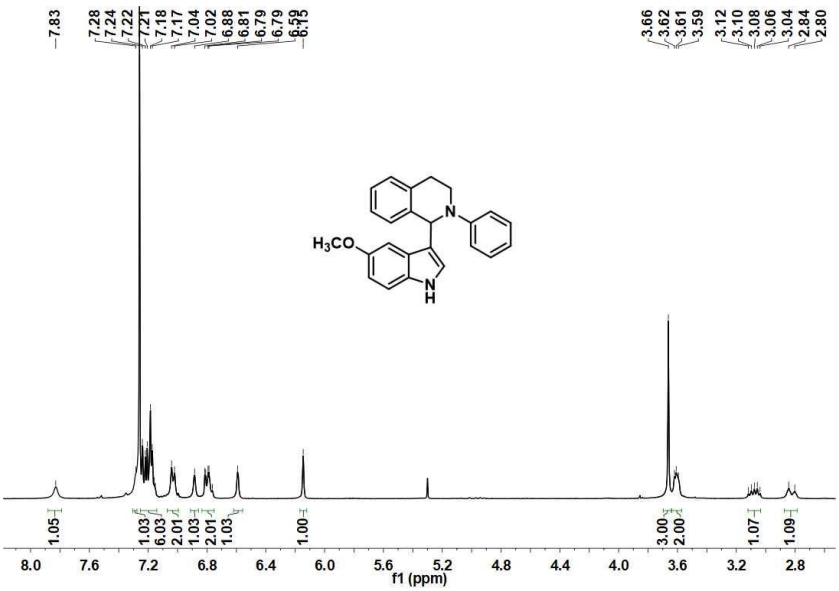

Fig. S31 ^{1}H NMR spectrum (400 MHz, $CDCl_3$, 298 K) of compound **3d**.

3e: ^{1}H NMR (400 MHz, $CDCl_3$, 298 K) δ 7.98 (s, 1H), 7.61 (s, 1H), 7.26 - 7.21 (m, 4H), 7.21 - 7.13 (m, 4H), 7.02 (d, *J* = 7.8 Hz, 2H), 6.82 (t, *J* = 6.9 Hz, 1H), 6.63 (s, 1H), 6.08 (s, 1H), 3.59 (dd, *J* = 7.8, 3.1 Hz, 2H), 3.12 - 3.00 (m, 1H), 2.80 (d, *J* = 15.6 Hz, 1H).

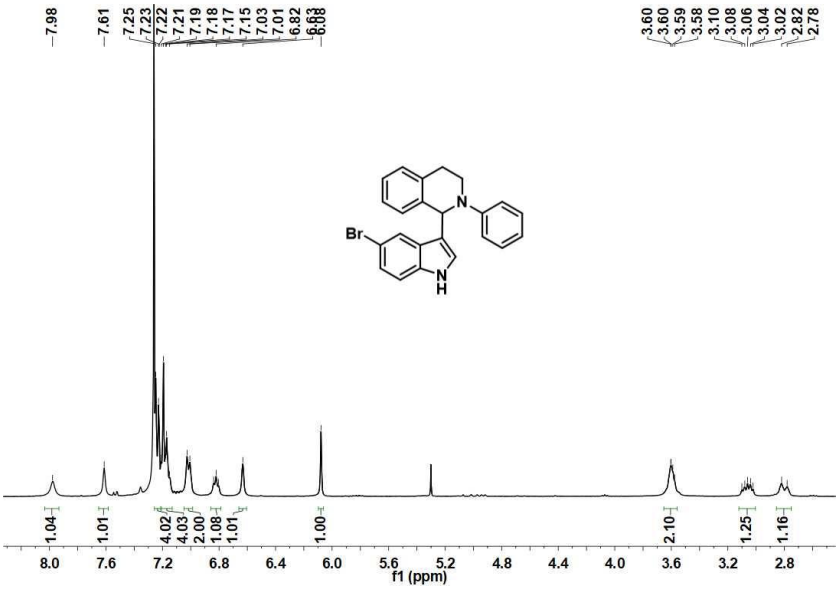

Fig. S32 ^{1}H NMR spectrum (400 MHz, $CDCl_3$, 298 K) of compound **3e**.

3f: ^{1}H NMR (400 MHz, $CDCl_3$, 298 K) δ 7.93 (s, 1H), 7.54 (d, *J* = 8.0 Hz, 1H), 7.32 (d, *J* = 8.1 Hz, 1H), 7.16 (dd, *J* = 12.7, 6.5 Hz, 5H), 7.04 (t, *J* = 6.5 Hz, 3H), 6.95 (d, *J* = 8.2 Hz, 2H), 6.61 (s, 1H), 6.11 (s, 1H), 3.59 (dd, *J* = 7.5, 4.2 Hz, 2H), 3.10 - 3.01 (m, 1H), 2.77 (dd, *J* = 13.0, 3.3 Hz, 1H), 2.26 (s, 3H).

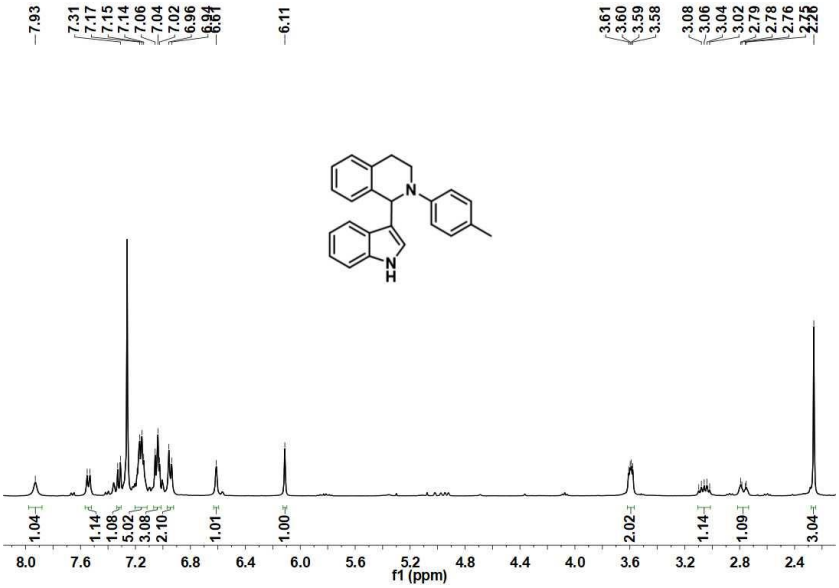

Fig. S33 ^{1}H NMR spectrum (400 MHz, $CDCl_3$, 298 K) of compound **3f**.

3g: ^{1}H NMR (400 MHz, $CDCl_3$, 298 K) δ 7.95 (s, 1H), 7.41 (s, 1H), 7.31 (d, J = 8.1 Hz, 1H), 7.21 - 7.12 (m, 5H), 6.99 (dd, J = 14.8, 7.2 Hz, 3H), 6.79 (d, J = 8.7 Hz, 2H), 6.59 (dd, J = 10.8, 4.7 Hz, 1H), 5.97 (s, 1H), 3.75 (s, 3H), 3.60 - 3.46 (m, 2H), 3.11 - 2.99 (m, 1H), 2.84 (dd, J = 19.9, 10.1 Hz, 1H).

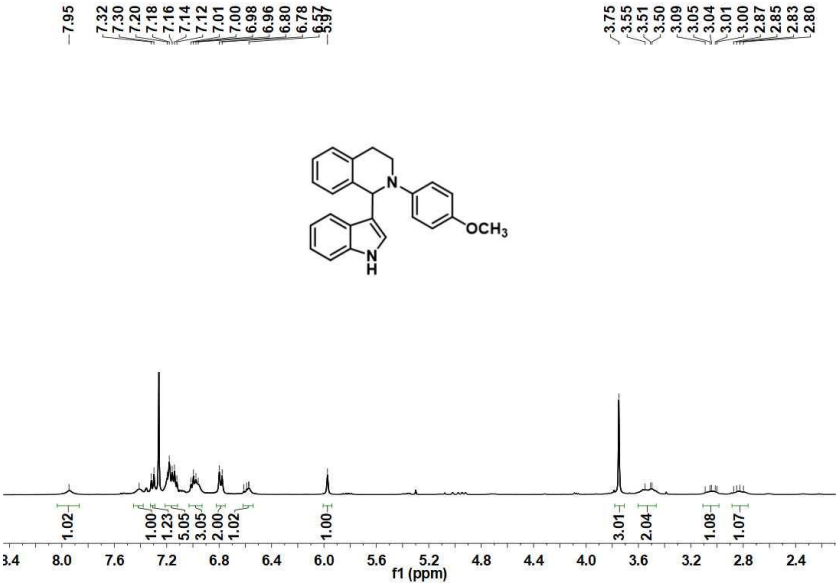

Fig. S34 ^{1}H NMR spectrum (400 MHz, $CDCl_3$, 298 K) of compound **3g**.

3h: ^{1}H NMR (400 MHz, $CDCl_3$, 298 K) δ 7.96 (s, 1H), 7.53 (t, J = 8.4 Hz, 1H), 7.35 - 7.27 (m, 4H), 7.18 (dd, J = 14.5, 6.4 Hz, 4H), 7.05 (t, J = 7.5 Hz, 1H), 6.90 (d, J = 7.1 Hz, 2H), 6.66 (s, 1H), 6.11 (s, 1H), 3.59 (dd, J = 16.9, 11.8 Hz, 2H), 3.11 - 2.99 (m, 1H), 2.84 (d, J = 19.5 Hz, 1H).

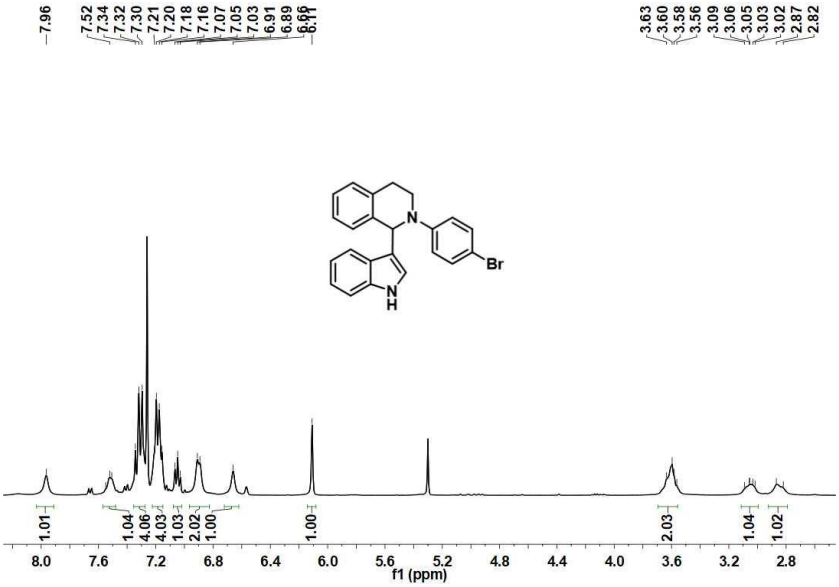

Fig. S35 ^{1}H NMR spectrum (400 MHz, $CDCl_3$, 298 K) of compound **3h**.

14. References

1 C. L. D. Gibb and B. C. Gibb, *J. Am. Chem. Soc.*, 2004, **126**, 11408-11409.

2 M. Hao, G. Sun, M. Zuo, Z. Xu, Y. Chen, X.-Y. Hu, and L. Wang, *Angew. Chem. Int. Ed.*, 2020, **59**, 10095-10100.

3 Y. Wang, N. Han, X.-L. Li, R.-Z. Wang, and L.-B. Xing, *ACS Appl. Mater. Interfaces*, 2022, **14**, 45734-45741.

4 K.-X. Teng, L.-Y. Niu, and Q.-Z. Yang, *Chem Sci*, 2022, **13**, 5951-5956.

5 P. K. Javvaji, A. Dhali, J. R. Francis, A. P. Kolte, A. Mech, S. C. Roy, A. Mishra, and R. Bhatta, *Front Cell Dev Biol*, 2020, **8**, 764.